

Prediction and Measurement of Multi-Tip Flare Ignition

Joseph D. Smith, Ph.D. and Ahti Suo-Anttila, Ph.D.,
Systems Analyses and Solutions, Owasso, Oklahoma, USA

Nigel Philpott and Scot Smith, Zeeco, Inc.
Zeeco Inc. Broken Arrow, Oklahoma, USA

ABSTRACT

Elevated multipoint flares represent a special class of flares capable of processing significant quantities of flare gas. A detailed computational fluid dynamics (CFD) model of an elevated multipoint flare has been developed using a proprietary flare modeling tool called C3d. This tool has been used to simulate the ignition phenomena for this particular flare for flare gas flow rates between 200 to 350 tons per hour (TPH). Simulation results have been directly compared to operating test data for this flare. Results demonstrate the ability of C3d to replicate the measured flame spread rate and reproduce the measured pressure wave generated during the ignition event. Based on this validation, the tool has been used to conduct over sixty separate simulations to investigate the ignition behavior for this flare. Results from these simulations clearly show the critical effect of ignition delay on the magnitude of the pressure wave generated on ignition. The main conclusion drawn from this analysis is that the ignition system's reliability to quickly ignite the flare gas above the flare tip is critical to safe operation. Predictions show that a 0.6 second ignition delay results in a significant pressure wave generated during flare ignition. Simulations at maximum flow rate (1350 TPH) exhibit explosive tendencies with pressure waves greater than one atmosphere. This confirms the conclusion that the flare must be operated with a continuous pilot to avoid and type of ignition delay. These results underscore the importance of the API recommended practice of continuous pilot operation for all large scale gas flares.

INTRODUCTION

This paper describes results from a series of computational fluid dynamics (CFD) simulations of an elevated multi-tip gas flare (see Figure 1) that is operated at nominal and maximum gas flow rates ranging from 300 – 1350 ton/hr (TPH). Results have been compared to field testing conducted to measure the pressure wave and flame front propagation velocity observed during ignition. The main focus of this paper is the CFD analysis of various ignition scenarios considering instantaneous ignition and delayed ignition to assess the potential impact of using a continuous pilot compared to a “discrete” ignition system (i.e., a flaming arrow).

The CFD tool used in this work simulates turbulent reaction chemistry coupled with radiative transport between buoyancy driven fires (i.e., pool fires, gas flares, etc.) and surrounding objects (i.e., wind fence, process equipment, etc.). The code provides “reasonably” accurate estimates of various risk scenarios including wind, % flame coverage, and thermal fatigue for a given geometry. Typical simulations generally require CPU times on the order of hours to a few days

on a “standard” windows (or LINUX) desktop workstation. Large Eddy Simulation (LES) is used to approximate turbulent mixing. The code used in this work is based on an earlier CFD tool called ISIS-3D [1-3]. ISIS-3D was previously validated for simulating pool fires to predict the thermal performance of nuclear transport packages [4-7]. ISIS-3D, originally developed at Sandia National Laboratory, has been commercialized into a new CFD tool called *C3d* which is specifically tailored to analyze large gas flare performance. *C3d* has previously been applied to large multipoint ground flares, air-assisted flares, and utility flares [8, 9] with new combustion models developed, implemented, and tested for typical flare gas including methane, ethane, ethylene, propane, propylene and xylene. *C3d* has been used to predict flare flame size and shape, estimate the smoking potential for a given flare design firing typical flare gas, and to estimate the radiation flux from the flare flame to surrounding objects. *C3d* simulations of flame height and flame-to-ground radiation have been validated by direct comparison to measured flame size, shape, and radiation measurements taken during single-burner and multi-burner tests conducted under no-wind and low-wind ambient conditions [9].



Figure 1 - Elevated multi-tip HP air flare firing natural gas

For the flare shown above, *C3d* predictions have been compared to test results previously collected to quantify the ignition behavior of the flare during nominal operating conditions (i.e., ~300 TPH under no-wind conditions). Test results included measured sound levels collected at four sample positions (see Figure 2) during ignition to estimate the pressure wave generated during ignition. High speed video was collected from two positions to estimate flame front velocity of the expanding flame ball during ignition. Pressure wave intensity was estimated from the flame front propagation velocity with the pressure magnitude inferred from an empirical correlation [6].

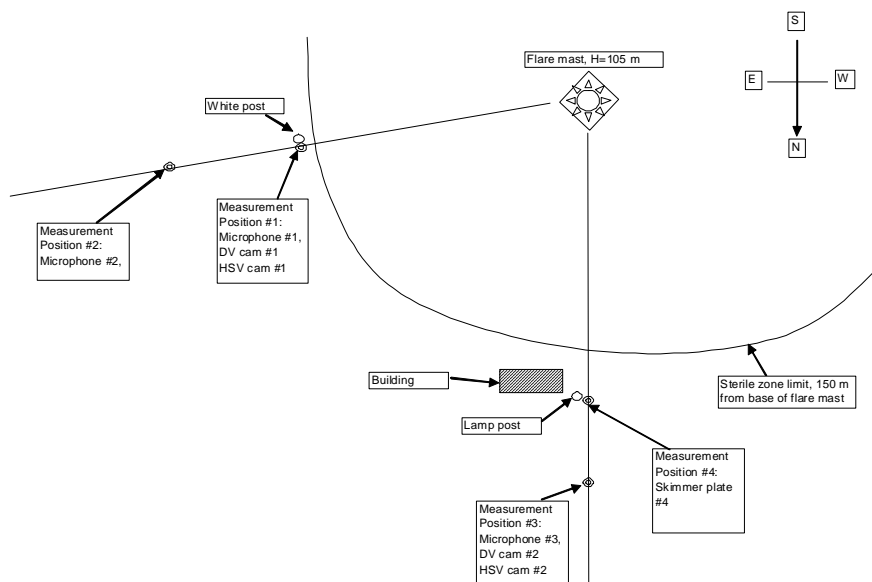


Figure 2 - Approximate measurement locations around the flare mast

TECHNICAL APPROACH

The approach used in this work was to model the flare and its surroundings with as many computational cells as reasonable, and vary the parameters associated with the combustion model such that the pressure and flame propagation best matched the experimental measurements. Those parameters that best matched the test data were then used to estimate the pressure wave intensity for the specific flow conditions.

To estimate the pressure wave intensity, a large computational volume of 20m long by 20m wide by 15 m high was considered. Since the flare dimensions are approximately 3.35 m square, the edges of the computational domain considered extended approximately 9 m beyond the edge of the flare. Since this was an elevated flare, the bottom of the computational domain considered as set at the level of the nozzle tips instead of ground level to reduce domain size and associated computational load for the simulations.

The computational domain was separated into two distinct regions. The first region was located just above the flare tip nozzles and was 7 m square in horizontal extent and 8 m high. This region used fixed horizontal cells with equal spacing (80 cells each 0.0875 m on a side). The vertical

dimension used a slowly varying grid structure 0.05 m cells at the nozzle tip and 0.14 m cells at the top of the central region for a total of 90 cells in the vertical direction. In all, the number of computational cells in the central “high resolution” region was 80 x 80 x 90 or 576,000 cells. The second region, surrounding the central region, used coarse, highly stretched cells to provide a buffer zone to the actual domain boundary. The number of cells in the buffer zone was 14 on both sides horizontally and 12 vertically for a total of 108 x 108 x 102 = 1,189,728 computational cells. The buffer zone provided a large distance from the edge of the computational domain so that the pressure boundary conditions were far removed from the flame so that they did not affect the estimated pressure in the igniting gas ball. During the course of the analysis, the grid was redefined several times to improve calculation results with the final grid, as described above, shown in Figure 3.

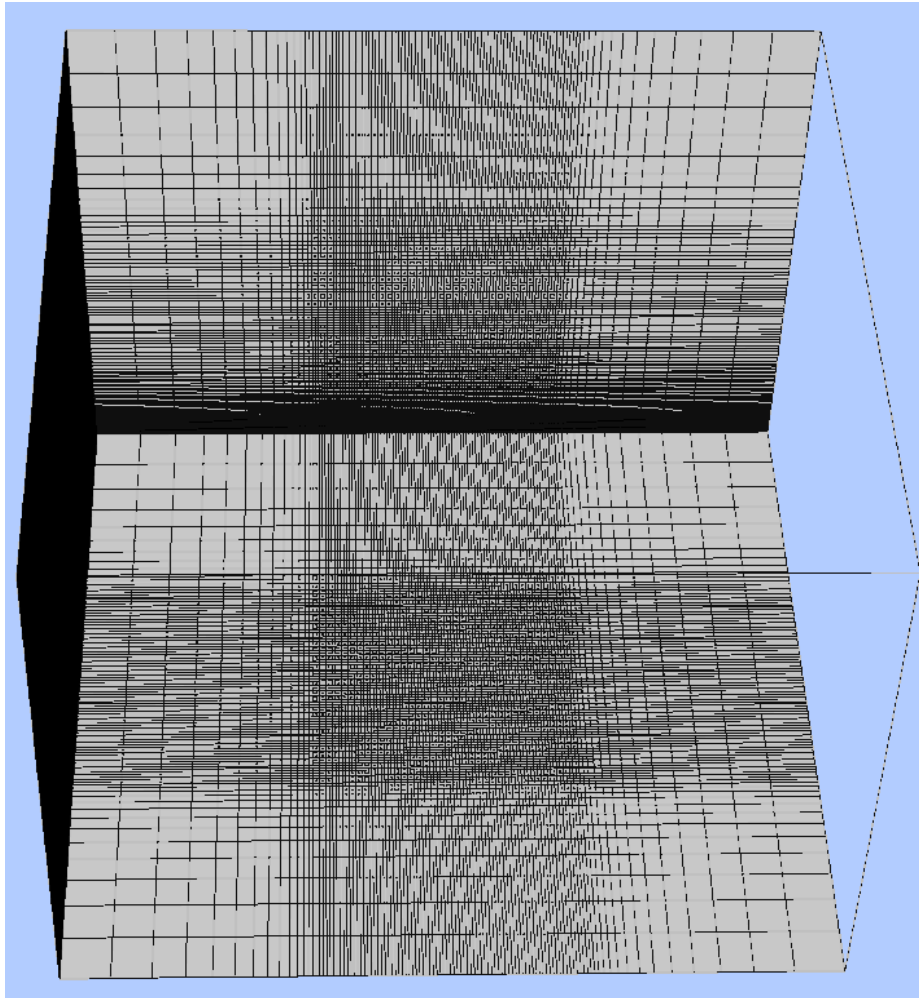


Figure 3 – Final grid structure used in the flare gas ignition analysis (fine grid in central region to resolve ignition ball; coarse surrounding grid to reduce effect of pressure boundary conditions on ignition phenomena)

The full complex flare structure was not included in the model to reduce the computational overhead required to analyze the ignition phenomena. Since the flare tip structure likely does not

affect the growth of the igniting ball (this behavior occurs well above the flare tip itself), this approximation was considered justified and appropriate. However the nozzle exits were included to act as a blockage to prevent air from being prematurely drawn into the natural gas jets. The blockage forced the air to mix with the gas jets by side infiltration only.

Flow exiting from a high speed jet has two distinct flow regimes including a constant velocity cone, surrounded by a surface where air is mixing with the gas in the cone as shown in Figure 4.

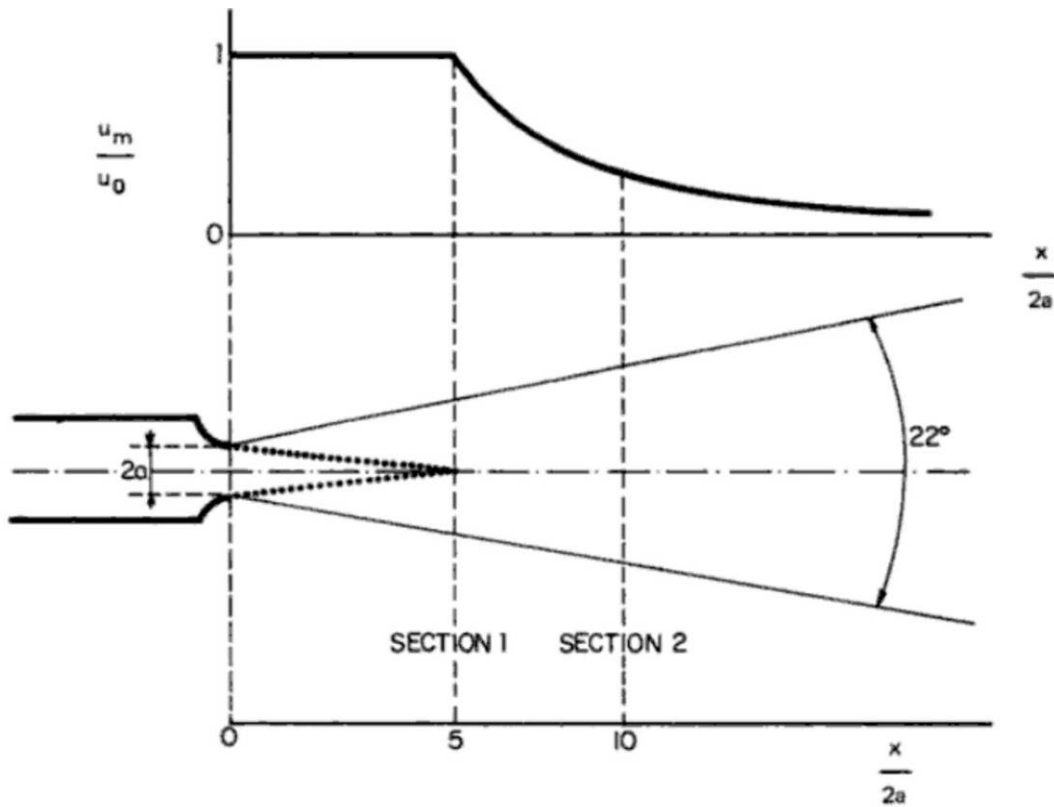


Figure 4 - Diagram of a free jet discharging into a calm atmosphere from Monnet [12]. The region outlined by dots is a constant velocity cone 5 nozzle diameters in length

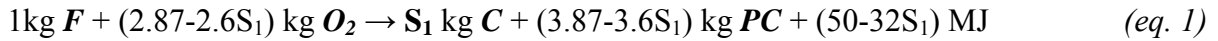
Since the computational cells used were a significant fraction of the nozzle diameter it would not be possible to resolve the shape and size of the nozzle or fluid exit cone. To appropriately resolve the mixing cone, a FORTRAN program was written that placed a large number of fluid sources along the surface of the cone. For the entire nozzle structure this worked out to be 7700 mass sources. The fluid sources inject natural gas at the correct velocity and mass rate as would be obtained if the exit cone were resolved by very fine computational cells. Using this approach, the flow from each individual nozzle was kept exactly identical (in the absence of any flow maldistribution to the individual nozzles).

An alternate approach was also used wherein fluid was injected from the top surface of all the structures that represent the nozzles. The total gas that was injected was adjusted to get 350 TPH for all the nozzles. However, the rate for each individual nozzle varied because the nozzle sizes

varied slightly depending upon the overlap of the square cells of the computational grid and the circular nozzle tips. Both approaches were found to give similar results.

COMBUSTION MODEL

The combustion model in *C3d* is a variant of Said et.al. [11]. The relevant species included in the hybrid combustion model are Fuel vapor (**F**) from flare tip, oxygen (**O₂**), products of combustion (**PC**) which include water vapor and carbon dioxide, radiating carbon soot (**C**), and non-radiating intermediate species (**IS**). The general combustion reactions involving these species include:



Eq. 1 describes incomplete fuel (**F**) combustion and produces soot (**S**) and products of combustion (**PC**) plus energy. The standard combustion soot stoichiometric parameter (**S₁**) is set as 0.05 but can be adjusted based on fuel type. For natural gas a value of 0.005 was used.

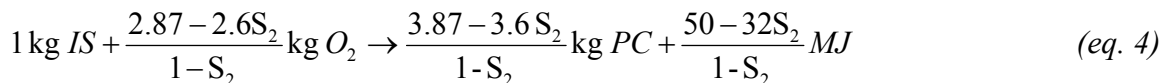
The endothermic fuel pyrolysis or cracking reaction (soot producing) consumes fuel (**F**) and energy and produces radiating carbon (**C**) plus the intermediate species (**IS**):



Eq. 2 includes the Cracking Parameter (**S₂**) which is set as 0.15 but can also be adjusted based on fuel type. Soot combustion is described by:



which consumes soot (**C**) and oxygen and produces carbon dioxide plus some energy. The Combustion of Intermediate Species is described by:



where the coefficients are selected so that complete combustion of soot (**C**) and intermediate species (**IS**) produce the same species and thermal energy as direct combustion of the fuel. The coefficients in the formula are mass weights, not moles.

The advantage of the three-step reaction is that the first reaction has a low activation energy, which allows the partial burning and heat release of the flare gas. This will maintain combustion since the partial heat released will allow the second reaction, which produces most of the heat and all of the soot, to occur. As in the previous combustion models developed for flare simulations [9], the flare gas Arrhenius combustion time scale is combined with the turbulence time scale to yield an overall time scale for the reaction rate. The characteristic time from the kinetics equation was combined with the characteristic turbulence time scale:

$$t_{\text{turb}} = C \Delta x^2 / \epsilon_{\text{diff}} \quad (\text{eq. } 5)$$

Where Δx is the characteristic cell size, C is a user input constant ($0.2E-4$), ε_{diff} is the eddy diffusivity from the turbulence model, and t_{turb} is the turbulence time scale, i.e. characteristic time required to mix the contents of a computational cell. The reaction rates are combined by simple addition of the time scales. This combustion model captures the eddy dissipation effects and local equivalence ratio effects. The reactions are all based on Arrhenius kinetics with:

$$\frac{df_{R_i}}{dt} = -C \left[\prod_i^N f_{R_i} \right] e^{-T_A/T} \quad (eq. 6)$$

where coefficients C and Activation Temperatures T_A are supplied for all reactions. The Arrhenius kinetics and turbulent mixing form the commonly used Eddy-Breakup (EBU) type combustion model.

The kinetics and turbulence models are combined by summing the characteristic time scales. In addition to these dynamic models, sequences of irreversible chemical reactions that describe the combustion chemistry are required. To minimize computation load, a minimum number of chemical reactions are used that fulfill the requirements of total energy yield and species consumption and production. From the basis of heat transfer, flame size, and air demand the details of the chemical reactions are not critical as long as the oxygen consumption is correctly balanced for a given fuel type. To this end, a multi-step chemical reaction model for natural gas was used to approximate the global reaction mechanism as shown in the equation below:

$$DX_1/dt = A_k * T_b * X_{1c} * X_{2d} \text{Exp}(-E_a/T) \quad (eq. 7)$$

Where A_k is the pre exponential coefficient, X_1 is the mole fraction of natural gas, X_2 is the mole fraction of oxygen, E_a is an activation temperature, T is the local gas temperature, and b , c and d are global exponents.

Global reaction kinetics are often used to model combustion as a single step in CFD combustion simulations. The coefficients and powers are fit to existing experimental data. Although it is possible to use a global reaction mechanism with the same coefficients as those which have been published elsewhere, this could be misleading because the coefficients were originally fit to experimental data chosen by other authors for a specific combustion experiment being modeled and it is well known that simulation results are sensitive to both the computational grid (cell structure and density) and the experimental data chosen by the original authors. A different computational grid or experiment would likely require a different set of reaction coefficients.

In the present work, the global reaction mechanisms of Duterque et. al. [13] and Kim [14] were chosen as starting points. However, these authors adjusted their global reaction coefficients to match “laminar” flame speed data. The combustion occurring in the gas flare being modeled in this work, flame speed is governed by turbulent mixing, not laminar flow, hence their original coefficients have limited applicability but do provide a good starting point. The coefficients associated with the activation temperature and the exponents on the mole fractions are based upon the physics of the reaction mechanism and therefore are not expected to be sensitive to local grid structure. However, that is not the case with the pre-exponential coefficient. Therefore,

to match reaction rates with measured combustion rates, only the pre-exponential coefficients were varied as a parameter in this effort to develop a validated combustion model.

The combustion model also depends upon turbulent mixing. Since the natural gas is injected as a pure species, the combustion is governed not only by chemical kinetics but also by turbulent mixing with air. The C3d code uses an LES formulation to approximate turbulent mixing, and that formulation has two proportionality coefficients, which were also varied as parameters in the combustion model development work. The first coefficient, ϵ , is a scale factor to the turbulence intensity as a function of the strain rates in the local fluid flow. The second coefficient, δ , is a time delay factor that is added to the kinetics rate coefficient to account for the delay in the mixing of combusting species in the computational cell.

The following table (see Table 1) shows the parameter selection used in this analysis. A_k is the value of the pre-exponential coefficient in SI units, ϵ is the dimensionless LES proportionality coefficient, and δ is a dimensionless turbulent mixing time coefficient.

Table 1- Parameters varied in Combustion Modeling tuning

Parameter Varied In Combustion Model Development	Parameter Value(s) Considered In Model Tuning
A_k	1.0e14, 2.5e14, 5.0e14, 1.0e15, ..., 5.0e17
ϵ	0.10, 0.15, 0.20, 0.25, 0.30, 0.35, 0.40
δ	1.0e-4, 5.0e-5, 1.0e-5, 5.0e-6, 1.0e-6

Other modeling variations were also included in this analysis. They included:

1. Computational grid size and number
2. Turbulence model, both zero equation and one- equation LES
3. Effect of nozzle structure, both with (jet cone) and without (nozzle surface)
4. Numerical upwind differencing
5. Time to ignition

MODELING ASSUMPTIONS

The following assumptions were utilized in modeling the elevated flare:

1. Combustion of the flare gas was approximated by the appropriate irreversible chemical reaction mechanism with specified kinetics (see above).
2. Thermal radiation was calculated using standard radiation models.
3. Ambient wind condition, flare gas inlet temperature and pressure, and radiation effects were set to match as closely as possible those measured in the flare tests.

Boundary Conditions

The Boundary conditions used were hydrostatic pressure on all boundaries. The only exception to using a hydrostatic boundary condition would be for cases where a cross wind was blowing and since no cross wind data was available this option was not used. The thermal and species boundary conditions were set to 300 K (27°C) and air composition respectively.

Physical and Numerical Sub-model Selection

To simulate fluid flow, the momentum solver was the C3d LES turbulence model as described above. The energy equation was utilized to capture the temperature changes due to combustion and mixing. The energy equation also included radiation effects.

The species equations were solved to keep track of the distribution and concentration of fuel, oxygen, intermediate species, soot, and products of combustion (CO₂ and H₂O). The combustion model was used to provide the species equations source and sink terms as a function of species concentrations, local gas temperature, and turbulent diffusivity.

C3d includes a series of models to predict flame emissivity as a function of molecular gas composition, soot volume fraction, flame size, shape and temperature distribution. In turn these variables depend upon solutions to the mass, momentum, energy and species equations. The radiation transport model is used not only to predict radiation flux on external (and internal) surfaces, but it also provides source and sink terms to the energy equation so that flame temperature distribution can be predicted.

Transient Calculation and Post-Processing Results

To set up the ignition conditions as they exist in the flare tests, the simulation was run with a ignited pilot and nitrogen gas injected through the flare tips at the same mass flow rate as the natural gas firing rate to achieve a steady state flow condition to improve computational stability and convergence. The simulation was then re-started with natural gas and allowed to self ignite from the burning pilot. Once ignition was achieved, the gas pressure was monitored at several locations (see Figure 5) to evaluate the magnitude of the ignition generated pressure wave. In addition to history plots of pressure at each location, contour plots of the pressure were at various time steps were also prepared. The contour plots (with time stamp) were used to estimate flame growth rate.

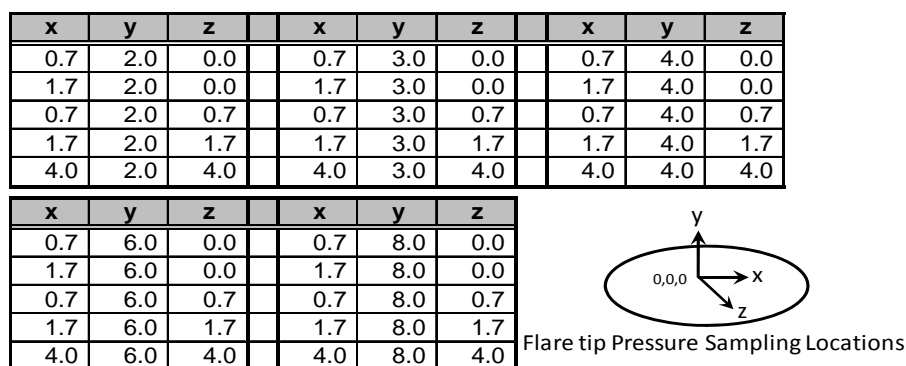


Figure 5 - Pressure Monitoring locations for Max flow case (Note: For pressure monitoring points, x and z are horizontal positions with x = 0 and z = 0 as the flare center and y is the height above the flare tip as shown in graphic)

Since a transient solver was used, all field variables fluctuate in time due to turbulence and the other non-linearity's in the equation system. However when examining any field variable, no gradual slope was observed - just short term fluctuations as expected in turbulent flows.

The convergence criteria chosen for the simulations were that the equation of state was always satisfied to within 0.1% or less at any location in the computational domain. Typically the convergence criteria was better than the maximum allowable since the time step constraint was limited by Courant conditions, which allows the flow field to be solved to a higher degree of accuracy.

RESULTS

Since the flare normally operates with a gas flow rate between 200 – 300 TPH, several cases were completed for this condition. Results from these simulations are presented and discussed below. In addition, the maximum flare flow condition is approximately 1350 TPH so several cases were also completed for this condition to analyze the ignition behavior for high flow condition. Results for the high flow condition are also presented and discussed below.

Low Flow Rate Results

The results of over 60 CFD runs indicate that the magnitude of the pressure pulse is primarily dependent upon ignition time with secondary effects from combustion kinetics and turbulence. These runs considered flow rates of 200 and 310 TPH. Although most runs were focused upon varying the combustion kinetics and turbulence parameters, many of these runs had a similar outcome, that is, the magnitude of the pressure pulse was approximately +30 to 40 millibars (mB) with the maximum pulse followed by negative pressures of between -10 to -20 mB. This outcome is somewhat surprising in that the combustion parameters were varied over a significant range and yet the magnitude of the peak pressures fairly similar. Figure 6 is a chart of the maximum and minimum pressures that resulted at three different elevations in forty-one different cases. Other cases were run, but a different computational grid was used so those cases are not included for consistency. Suffice it to say that the other cases not shown had similar results.

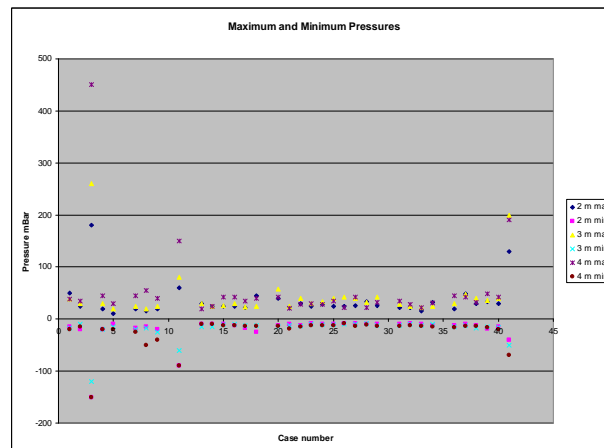


Figure 6- The maximum and minimum pressure, in millibars, encountered during the ignition phase of the natural gas burners at 3 different elevations above the nozzles

The runs that had combustion delays exhibited higher pressure waves overall. One particular case (Case #3) had an overpressure as high as one-half atmosphere (approximately 7 psig),

although that case did have extensive numerical fuel-air mixing due to large computational cell sizes in the region where the explosion initiated (8 m above the nozzles).

Another case (Case #41) was designed to have an ignition delay. The natural gas jets were turned on for 0.25 sec prior to igniting the pilot. After ignition, the pilot flame grew and ignited the flare gas at approximately 1 sec. The resulting flame ball had significantly higher pressures than nearly all the other cases considered, except those that had ignition delay for one reason or another.

Since a number of calculations were made not all of these results will be shown. Instead, only results that most closely matched the previous test results are presented.

The final chemical kinetics coefficients selected as providing the “best” fit to comparison to the ignition tests were: $A_k = 5.0e16$, $T_a = 20098$, $b = 0.5$, $c = 1$, and $d = 1$. The turbulence parameters selected were: $\epsilon = 0.2$ and $\delta = 1e-5$.

These kinetics and turbulence parameters were not the highest values tested (i.e. fastest kinetics and most rapid mixing). Cases with higher values did not always result in higher pressures because high values also lead to combustion in non-ideal mixtures. The regions directly above the nozzles had regions that were either fuel rich or fuel lean (non-ideal combustion conditions). Values of high kinetic coefficients burn the components in the rich and lean zones almost completely which often does not yield much heat due to non-ideal stoichiometry. Non-ideal burning deprives additional fuel-air mixing that could lead to later burning with higher temperatures and pressures.

Increasing the turbulence scale factor does improve mixing, however is also suppresses the natural fluid oscillations in the turbulent jets which an LES formulation is designed to model. Therefore, the scale factor was not allowed to exceed twice the recommended value of 0.2.

Figure 7 shows a time history plot of the local gas pressure for a typical case at 4 m elevation above the nozzles. The results are slightly filtered where each point represents an average of 4 time steps. Without filtering, pressure at isolated locations and single time steps often displayed pressure peaks representative of ideal combustion conditions (see Figure 8). These isolated peaks were not considered to be representative of the experimental measurements since they often occur only for a single time step (<0.1 ms) which would be too fast for the test equipment used to accurately monitor. Filtering was used to insure that the pressure histories were representative of large regions and times which would be more consistent with pressure histories that were inferred from the flame velocity measurements.

As shown, the pressure change (maximum – minimum) reaches approximately 50 mB or more, which is the same as that reported by Wilkins [10]. The time between the maximum and minimum pressure is on the order of 16 ms, which corresponds to a sound frequency of approximately 60 HZ.

Figure 9 and Figure 10 show pressure histories typical of delayed ignition. Figure 11 shows the pressure is variable with many local high pressure peaks. The highest pressures are often

observed to form on the outer edge of the growing flaming ball. The minimum pressures are observed to be at the center of the flaming ball after the high pressure had propagated outward. Figure 12 shows three different horizontal slices of flame temperature at 4 m elevation above the nozzles. The flame as shown grows in fingers outward from the ignition point as it propagates between the jets, as though the jets acted as solid material blocking flame growth. Eventually the flame encompasses the entire volume.

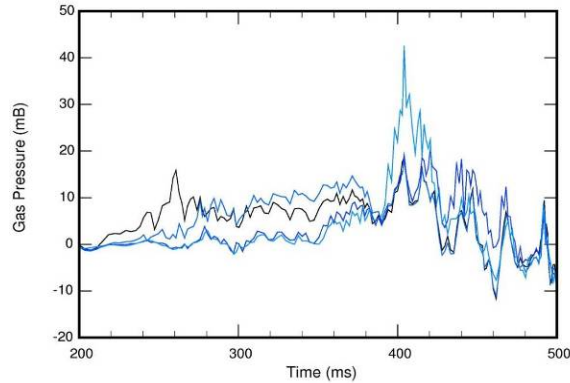


Figure 7- Case 18 pressure histories at 4 m elevation above the nozzles and various horizontal distances from flare centerline

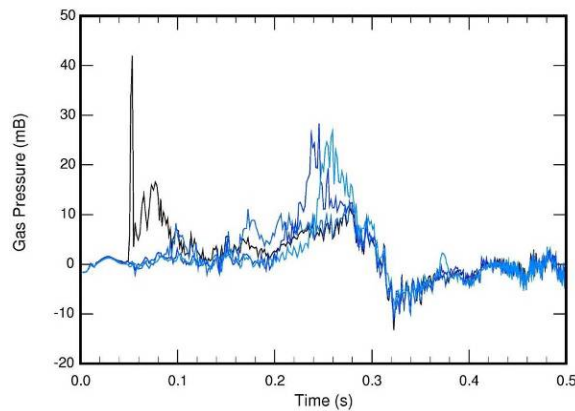


Figure 8- Case 37 pressure histories at 4 m elevation above the nozzles and various horizontal distances from flare centerline

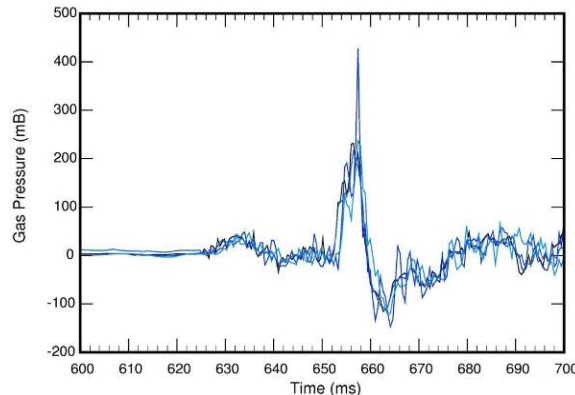


Figure 9 - Case 3 pressure histories at 4 m elevation above the nozzles and various horizontal distances from flare centerline. This case had delayed ignition

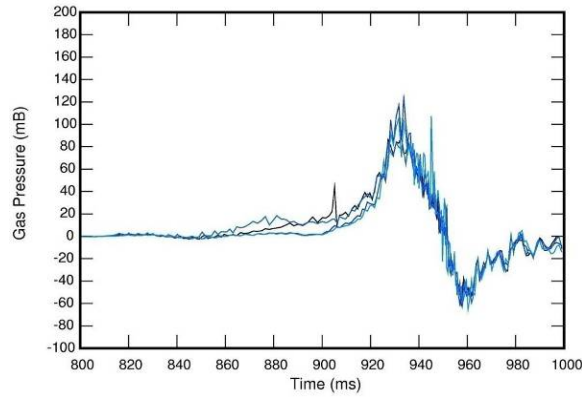


Figure 10 - Case 41 pressure histories at 4 m elevation above the nozzles and various horizontal distances from flare centerline. This case was designed to have delayed ignition

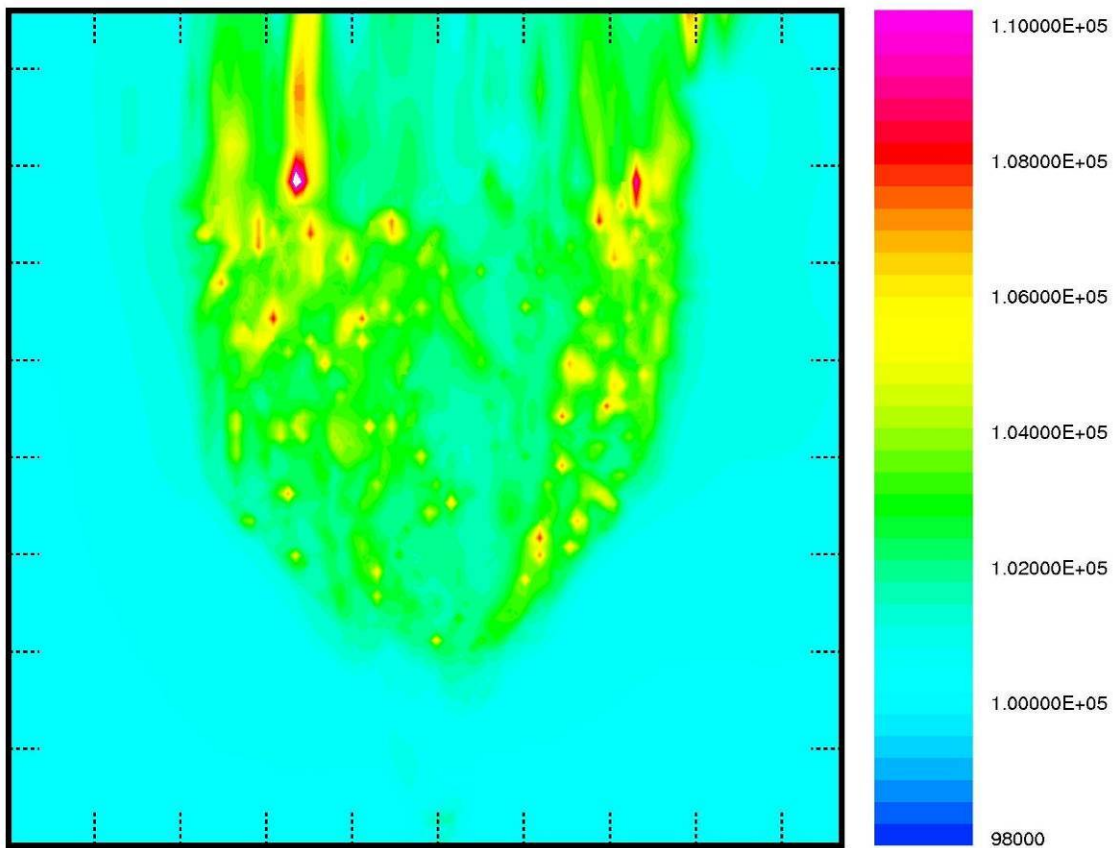


Figure 11 - Contour plot of pressure for Case 18 during “growing flame ball” phase of ignition. The pressure shown in SI units where $1.01E5 \text{ Pa} = 1 \text{ atmosphere}$

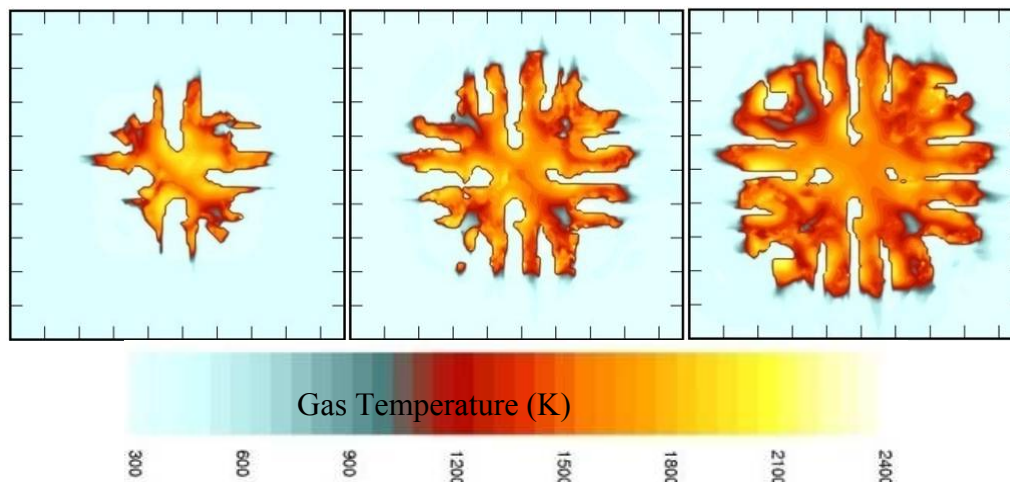


Figure 12 - Horizontal temperature contour on slice through flame ball at 4 m elevation: a) beginning phase of ignition, b) mid-point of ignition, and c) near end of ignition

The flame propagation velocity can be derived from two successive contour plots in Figure 12. Each tic mark in the plot corresponds to a 1 meter spatial distance. The time between any two plots is 30 ms. Dividing the flame propagation distance by the time between frames yields a propagation velocity of approximately 33 m/s depending upon what part of the flame being considered. The flame propagation velocity reported by Wilkins [10] was 50m/s, however examining video data from their experiments revealed that the actual growth rate was more likely between 40 and 44 m/sec. It appears that they neglected to subtract the initial ball diameter when calculating the growth rate.

Figure 13 shows selected frames from an animated sequence that better illustrates flare ignition, development of the growing flame ball, and the final burning flare flame. The pink structures at the bottom of the figure represent the nozzle tips. The view shown is from below the flare looking up. Figure 14 shows selected frames from an animated sequence of flare ignition when ignition has been delayed between 0.3 to 0.6 sec. For this case of ignition delay, a pressure wave of approximately 7 psig was developed which indicates the potential overpressure condition that may result from ignition delay.

FULL FLOW RATE RESULTS

Although the flare being analyzed normally operates at the low flow rate discussed in the previous section, on some occasions this flare may operate at flows up to approximately 1350 TPH. Given the over pressure condition that was predicted to occur for ignition delay during nominal flow, a second set of simulations were performed to assess the impact that operating at higher flow rates with ignition delay might produce. For these simulations, the previous CFD mesh was refined and extended to a thirty meter cube with 124 cells in the x-direction (domain width), 102 cells in the y-direction (domain height), and 124 cells in the z-direction (domain length) for a total of 1,568,000 cells. This mesh also included a fine and variable grid within the 8 m wide by 8 m long by 15 m high cube where the flare flame and plume was expected to exist during the higher flow conditions. Outside of this refined region, the mesh included a variable coarse grid to capture the air in-flow from the surrounding regions.

For these simulations, the pilot was ignited at the same time as the natural gas was injected into the burner tips. For all simulations, the pressure was monitored at the five points described earlier (see Figure 5). Results from a simulation with no ignition delay are shown in Figure 15 to Figure 17. For the full-rate cases, ignition occurs early with a max peak pressure of about 200 mB and a negative pressure following the peak pressure of between 50 and 100 mB. Results for a simulation with 250 ms ignition delay during which natural gas was sent through the flare tips and then ignited are shown in Figure 18 and Figure 19. For this case, the max peak pressure continues to grow until the code fails, since the code is not designed to simulate shock waves. After approximately 220 ms, pressure at all elevations exceeds 2000 mB with no negative pressure trailing the flame front. This prediction seems to indicate that the pressure front generated by the reaction front is trailing a shock wave as is the case in detonations. This prediction follows expected behavior based on results from ignition delay for a nominal flow rate. Two subsequent contour plots of gas temperature (see Figure 20) spaced 5 ms apart with tick marks on each plot spaced 1 m apart indicate the flame growth rate is approximately 600 m/s. This result supports the conclusion that firing the flare in this maximum flow condition coupled with an ignition delay leads to a detonation as opposed to the earlier predicted deflagrations. For the ignition delay maximum flow case, the pressure builds to more than 2000 mB after ignition until the code fails after approximately 220 ms. Comparing both the no-ignition delay case and the delayed ignition case, the strong effect of flow rate is clearly shown.

SUMMARY AND CONCLUSIONS

A study of the ignition characteristics of a natural gas flare was undertaken to assess the resulting pressure that might develop when the flare is ignited. A CFD model was created and approximately 60 runs were made for low flow conditions (200 – 310 TPH) by varying combustion kinetics, turbulence and other parameters that have an effect on the flame ball pressure. For the low flow conditions, the single most important parameter for predicted over pressure was the ignition delay. When the flare was ignited immediately, the predicted over pressures were in the range of 20 to 40 mB. When ignition was delayed, the simulations indicated that a large over pressure wave developed. In one case, a predicted pressure wave of approximately 7 psig (1/2 atmosphere) developed.

Several simulations were also completed for a high flow condition of 1350 TPH. For the peak flow condition, simulations were performed for both a no-ignition delay situation and a 250 ms ignition delay situation. For the peak flow cases, the mesh was expanded and refined in an attempt to better capture the evolving flame. For these cases, the grid contained approximately 1.6 million cells with variable spacing in the near flame region. Similar to the nominal flow condition, a significant pressure wave with explosive tendencies was predicted for the ignition delay situation. For all high flow cases considered, the predicted peak pressure developed into a detonation condition with flame velocities greater than 600 m/s and peak pressure greater than two atmospheres. It should be noted that for these cases, the code failed at this point as it was not designed to analyze shock waves and/or detonations.

Based on results from the normal and peak flow conditions, it is recommended that a continuous pilot based ignition system be used to ensure safe flare operation during ignition as recommended by API guidelines.

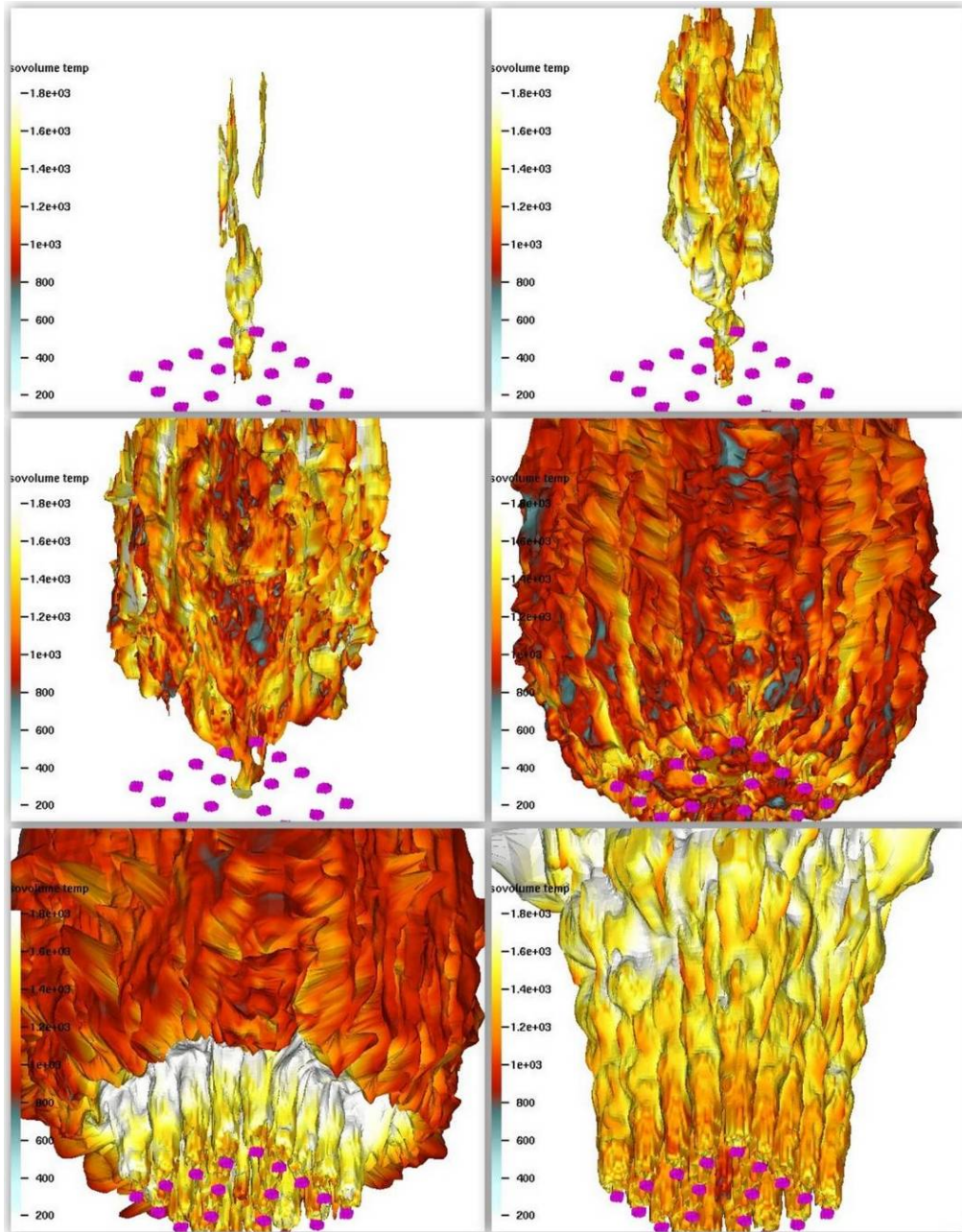


Figure 13 - Three-dimensional image of the growing flame ball

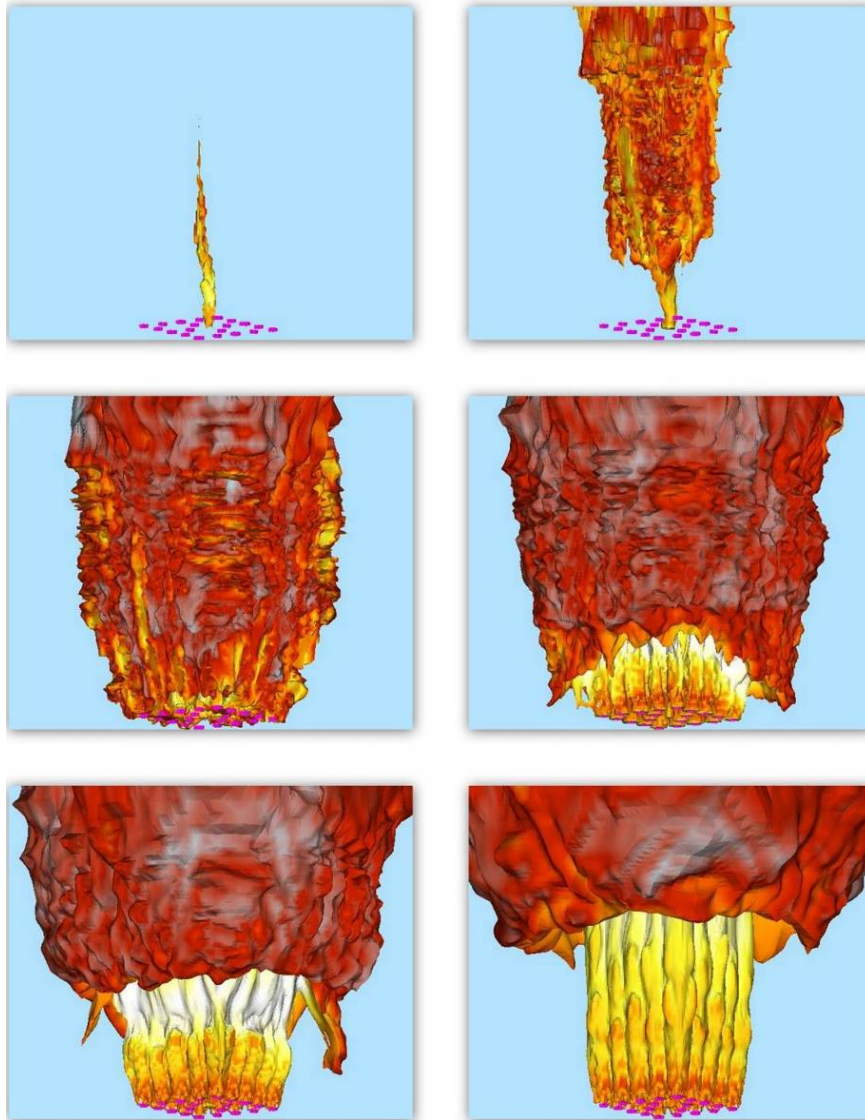


Figure 14 - Dimensional Image of a growing flame-ball with delayed ignition

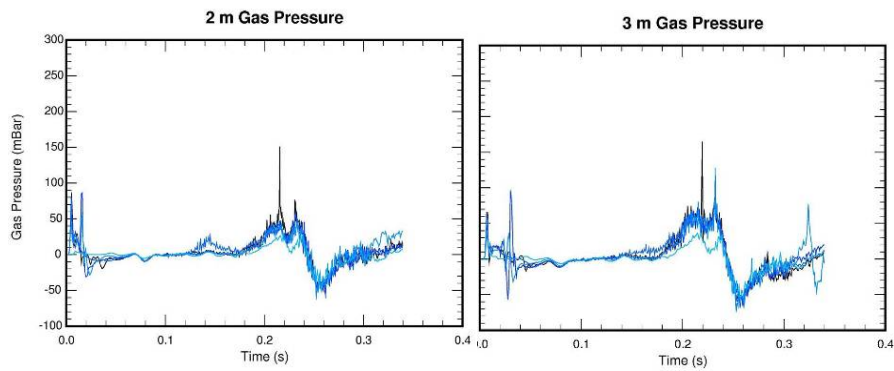


Figure 15 – Pressure histories at 2 m and 3 m elevation above flare tip at several horizontal distances from flare centerline with “No ignition delay” at full rate

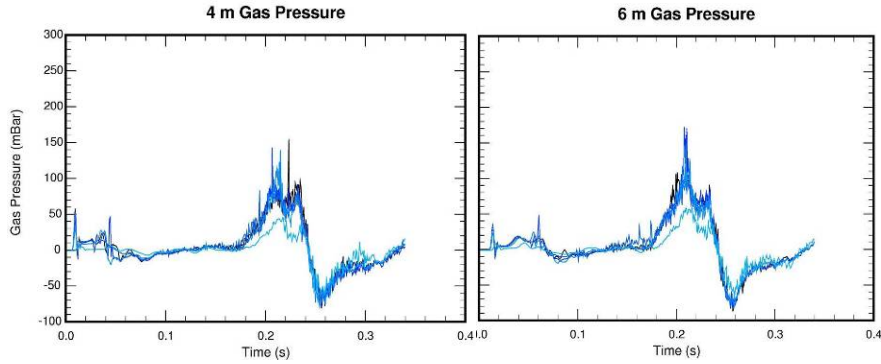


Figure 16 - Pressure histories at 4 m and 6 m elevation above flare tip at several horizontal distances from flare centerline with "No ignition delay" at full rate

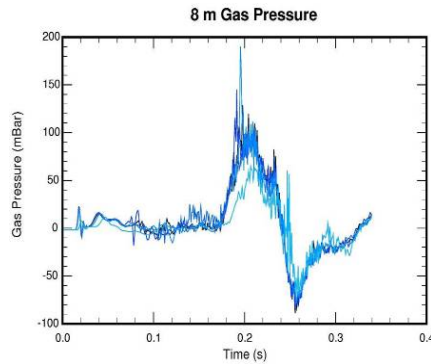


Figure 17 - Pressure histories at 8 m elevation above flare tip at several horizontal distances from flare centerline with "No ignition delay" at full rate

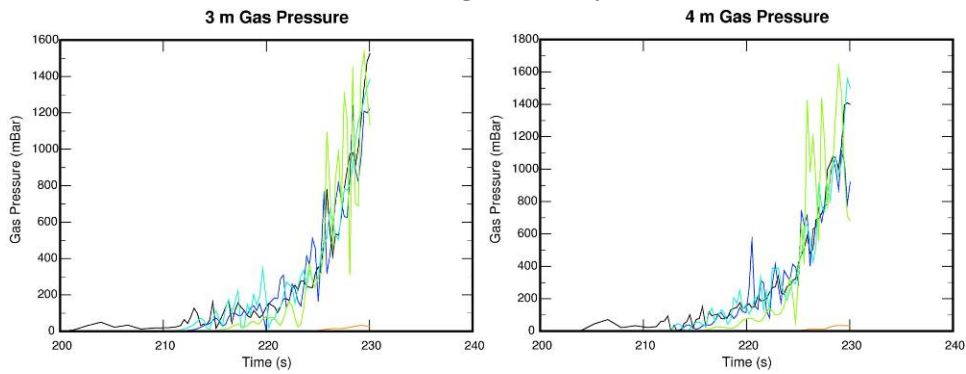


Figure 18 - Pressure histories at 3 m and 4 m elevation above flare tip at various horizontal distances from flare centerline for "250 ms ignition delay" at full rate

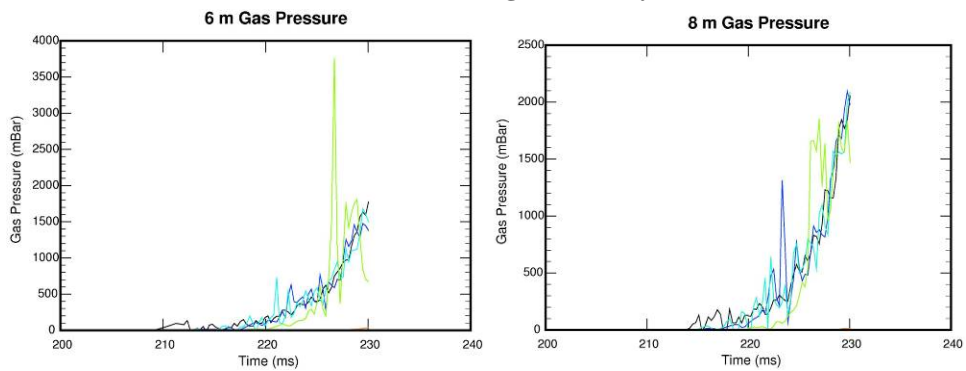


Figure 19 - Pressure histories at 6 m and 8 m elevation above flare tip at various horizontal distances from flare centerline for "250 ms ignition delay" at full rate

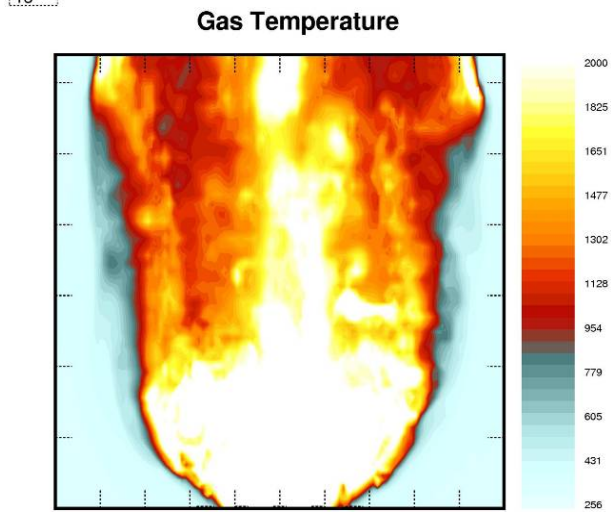
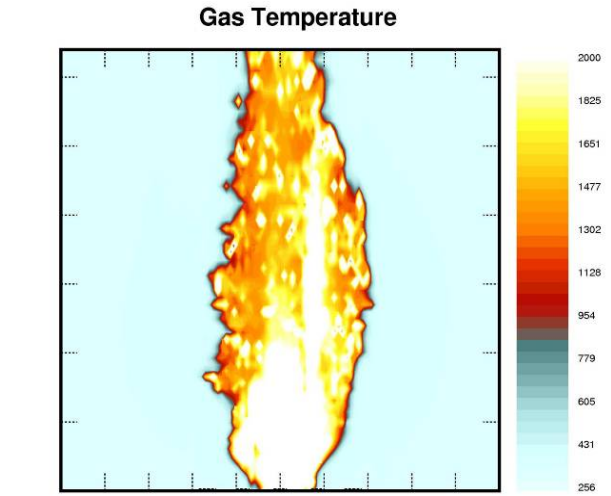


Figure 20 - Subsequent contours of gas temperature 5 ms apart. Each tick mark on the contours is spaced 1 m apart. Given this, the calculated flame speed is 3 m in 5 ms or 600 m/s

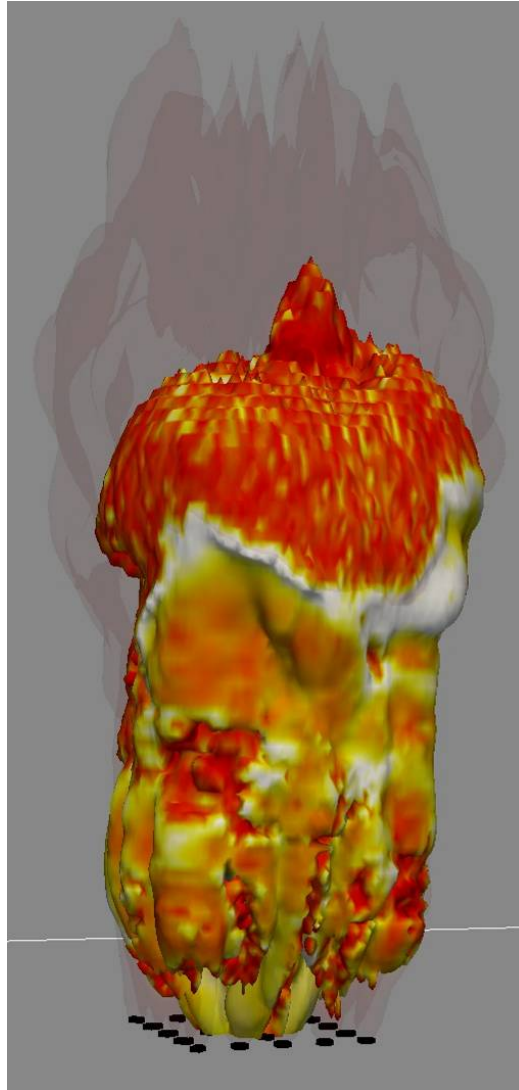


Figure 21 - Imposed predicted flame shapes from subsequent time steps showing flame growth

REFERECNES

1. Suo-Anttila, A., Wagner, K.C., and Greiner, M., **2004**, "Analysis of Enclosure Fires Using the Isis-3DTM CFD Engineering Analysis Code," *Proceedings of ICONE12, 12th International Conference on Nuclear Engineering*, Arlington, Virginia USA, April 25-29.
2. Greiner, M., and Suo-Anttila, A., **2004**, "Validation of the ISIS Computer Code for Simulating Large Pool Fires Under a Varsity of Wind Conditions," *ASME J. Pressure Vessel Technology*, Vol. 126, pp. 360-368.
3. Greiner, M., and Suo-Anttila, A., **2003**, "Fast Running Pool Fire Computer Code for Risk Assessment Calculations," presented at the *ASME International Mechanical Engineering Congress and Exhibition*, November 15-21, 2003, Washington, DC.

4. Greiner, M, Are, N., Lopez, C., and Suo-Anttila, A., "Effect of Small Long-Duration Fires on a Spent Nuclear Fuel Transport Package," *Institute of Nuclear Materials Management 45th Annual Meeting*, Orlando, FL, July 18-22, **2004**.
5. Society Fire Protection Engineers, **1995**, *Fire Protection Engineering*, 2nd Edition, National Fire Protection Association Publication.
6. Greiner, M., and Suo-Anttila, A., **2006**, "Radiation Heat Transfer and Reaction Chemistry Models for Risk Assessment Compatible Fire Simulations," *Journal of Fire Protection Engineering*, Vol. 16, pp. 79-103.
7. Fuss S.P., A. Hamins. **2002**, "An estimate of the correction applied to radiant flame measurements due to attenuation by atmospheric CO₂ and H₂O", *Fire Safety Journal*, Vol. 37, pp. 181-190.
8. Suo-Anttila, A., Smith, J.D., "Application of ISIS Computer Code to Gas Flares Under Varying Wind Conditions," *2006 American Flame Research Committee International Symposium*, Houston, TX, October 16-18 (2006).
9. Smith, J.D., Suo-Anttila, A., Smith, S.K., and Modi, J., "Evaluation of the Air-Demand, Flame Height, and Radiation Load on the Wind Fence of a Low-Profile Flare Using ISIS-3D," *AFRC-JFRC 2007 Joint International Combustion Symposium*, Marriott Waikoloa Beach Resort, Hawaii, October 21-24, (2007).
10. Wilkins B. "Statoil Flare Ignition Tests," Kollsnes, 26/8-09. CMR Gexcon Technical Note November (2009).
11. Said, R., Garo, A., and Borghi, R., "Soot Formation Modeling for Turbulent Flames," *Combustion and Flame*, Vol 108, pp. 71-86 (1997).
12. Monnot, G. Principles of Turbulent Fired Heat. Edition Technips, Paris (1985).
13. Duterque J., Roland B., Helene T., "Study of Quasi-Global Schemes for Hydrocarbon Combustion," *Combustion Science and Technology*, 26 (1-2), 1-15 (1981).
14. Kim I. K., Maruts K. "A Numerical Study on Propagation of Premix Flames in Small Tubes," *Combustion and Flame*, 146, 283-301 (2006).